TR－A－0133

Stability Constraints for the Equilibrium-Point Hypothesis

Menashe Dornay, Ferdinando A. Mussa-Ivaldi, Joseph McIntyre and Emilio Bizzi

1992. 2. 24

ATR視聴覚機構研究所

〒619-02 京都府相楽郡精華町光台2-2　☎07749-5-1411

ATR Auditory and Visual Perception Research Laboratories

2-2, Hikaridai, Seika-cho, Soraku-gun, Kyoto 619-02 Japan

Telephone: +81-7749-5-1411
Facsimile: +81-7749-5-1408

Stability Constraints for the Equilibrium-Point Hypothesis.

Menashe Dornay
Cognitive Processes
Department,
ATR, Kyoto,
Japan.

Ferdinando A. Mussa-Ivaldi
Joseph McIntyre
Emilio Bizzi
Department of Brain
and Cognitive Sciences,
MIT, USA.

Running head: Stability Constraints

Key words: Equilibrium point, Arm, Posture, Movement, Stability, Moment-arm, Muscle.

This work was supported by NIH grants NS09343 and AR26710 and by ONR grant N00014/88/K/0372 to E. Bizzi and F.A. Mussa-Ivaldi, and a Fairchild Fellowship to J. McIntyre. M. Dornay, who worked on this project both at MIT and at ATR, was supported at MIT by NIH fellowship 1-F05-TWO4042-01 and a Fairchild fellowship. M. Dornay would like to thank Drs. M. Kawato, K. Nakane and E. Yodogawa, ATR Auditory and Visual Perception Research Laboratories, for their continuing support.

Send correspondence to: Menashe Dornay, Cognitive Processes Department, ATR, Auditory and Visual Perception Research Laboratories, Sanpeidani, Inuidani, Seika-cho Soraku-gun Kyoto 619-02 Japan. (Fax +81-7749-5-1408).

*This manuscript was submitted to "Journal of Motor Behavior", theme issue on the control of arm and hand posture and movement, to be published in 1993.

Abstract

We have investigated the relation between static stability of a limb and the equilibrium-point hypothesis. Mathematically, the equilibrium-point control is equivalent to establishing a mapping between the command signals delivered to the muscles and the equilibrium configurations of a limb. A condition for this mapping to be possible is that the limb is stable across the workspace. We analyzed how this condition may be translated into precise biomechanical constraints for single- and multi-joint limbs. The satisfaction of these constraint is necessary for the equilibrium-point hypothesis to be a viable control paradigm.

Stability Constraints for the Equilibrium-Point Hypothesis

In order to generate purposeful motor behaviors, the brain must be able to perform and represent a variety of tasks ranging from the maintenance of posture to the generation of planned trajectories and the control of interactions with the environment. A number of investigators (Feldman, 1966; Kelso & Holt, 1980; Bizzi, Accornero, Chapple & Hogan, 1984; Hogan, 1984; Mussa-Ivaldi, Hogan & Bizzi, 1985) have suggested that the ability to maintain stable postures may be a building block for more complex behaviors. This idea is usually referred to as the *equilibrium-point hypothesis.*

The equilibrium-point hypothesis is based upon the observation that muscles behave like tunable springs (Rack and Westbury, 1969). At any fixed level of neuromuscular activation, the isometric tension developed by a muscle is a function of the muscle's length. Furthermore, the muscles acting upon a joint are organized in agonist/antagonist configurations. Thus, at any level of neuromuscular activation a limb's equilibrium configuration is achieved when the opposing torques generated by agonist and antagonist muscles cancel each other. If the limb is displaced by some external perturbation, the elastic muscle properties generate a net restoring torque which tends to bring the limb back to the original posture.

According to the equilibrium-point hypothesis, the central nervous systems generates movements by a gradual change in the equilibrium posture: at all times during the execution of a movement the neuromuscular activity defines a stable posture which acts as a point of attraction in the configuration space of a limb (Hogan, 1984). We investigated this crucial relation between postural stability and the equilibrium-point hypothesis. Our findings indicate that the

spring-like behavior of the muscles is not sufficient to ensure the stability of a limb at equilibrium. Limb stability is critically influenced by the geometrical arrangement of the muscles and, in particular, by their position-dependent moment arms. In this respect, the equilibrium-point hypothesis is a falsifiable theory: it is a viable control hypothesis if and only if some specific geometrical constraints are satisfied by the biological design of the musculoskeletal system. We investigated these geometrical constraints both analytically and by designing mathematical models of single-joint and multi-joint limbs.

Static Stability and Stiffness Eigenvalues

A limb is at an equilibrium posture when it is at rest, no external force acts on it and the net torque produced by the muscles is zero. An additional characterization of posture is offered by the concept of static stability. In general, a limb is statically stable when the pattern of torques induced by an externally-imposed displacement tends to restore the equilibrium posture. This concept is more rigorously defined by a condition on the stiffness tensor. Let the limb kinematics be described by a set of N generalized coordinates, $q_1, q_2, \ldots, q_N$. With this notation, a configuration of the limb is an array, $q = [q_1, q_2, \ldots, q_N]^T$. Accordingly, a generalized force is the vector $Q = [Q_1, Q_2, \ldots, Q_N]^T$. In a first approximation, biological limbs can be described as open chains of segments connected by rotational joints. In this case, the generalized coordinates are joint angles and the generalized forces are joint torques. The stiffness tensor in generalized coordinates, R, transforms an infinitesimal change of configuration into a change of generalized torque:

$$dQ = Rdq \tag{1}$$

This tensor is numerically represented by a $N \times N$ square matrix, R:

$$[R]_{i,j} = \frac{\partial Q_i}{\partial q_j}.$$

A necessary and sufficient condition for local stability about an equilibrium configuration is that all the eigenvalues of R have a negative real part (Ogata, 1970). We will restrict our analysis to statically conservative systems. For this type of systems, the stiffness tensor is symmetric and has real eigenvalues.[1] Therefore, the requirement of stability is reduced to the condition that all the eigenvalues of R are negative.

The restriction to statically conservative systems is consistent with the observation of symmetry in the stiffness tensor measured during the maintenance of multi-joint arm posture by human subjects (Mussa-Ivaldi et al., 1985). The symmetry of the stiffness tensor is relevant to the stability of an arm in contact with a mechanically passive environment (Colgate & Hogan, 1989). Loosely speaking, a system is passive when it cannot deliver more energy than what it has received. Recent theoretical investigations have demonstrated that a necessary and sufficient condition for coupled stability with a passive environment is that the arm itself behaves as a passive system at any fixed value of the motor commands (Colgate, 1988). An arm with a non-symmetric stiffness would not act as a passive system: it would either absorb or generate mechanical work in a quasi-static cyclical motion.[2]

Stiffness Transformations

Muscles are the controllable source of effort and stiffness for biological limbs. In a static (isometric) condition, muscles behave like *tunable springs* (Rack & Westbury, 1969). At any level of neuromuscular activation the iso-

metric force developed by a muscle is a function of the muscle's length. For a wide range of physiological lengths, the tension developed by a muscle during a stretch counteracts muscle's elongation ("muscles pull") and increases in amplitude with increasing stretch amplitudes. This behavior is tunable because a change in neural activation affects the length-tension curve smoothly, without drastically changing its shape. Mathematically, these observations are summarized by stating that the isometric tension, f developed by a muscle is a continuous differentiable function of the muscle's length, l, and input, u:

$$f = f(l, u). \tag{2}$$

Also, for a wide range of lengths the muscle stiffness, $k = \frac{\partial f}{\partial l}$ is negative.

Several muscles act on each joint in an agonist/antagonist configuration. Geometrically, the contribution of the muscles to the joint stiffness matrix is derived from a coordinate transformation. Let us consider a set of M muscles operating on N generalized coordinates ($M > N$). The lengths of these muscles define an M-dimensional space in which a generic point is given by the array $l = [l_1, l_2, \ldots, l_M]^T$. The kinematics of the limb determines a value of l for each value of q through the map:

$$l = \phi(q) \tag{3}$$

The local Jacobian of this map, $\mu = \frac{\partial \phi}{\partial q}$, is a rectangular, $M \times N$ matrix whose element i, j defines the moment arm of the i-th muscle with respect to the j-th joint angle.

Given a vector of muscle forces, $f = [f_1, f_2, \ldots, f_M]^T$, the corresponding joint torque vector, Q, at a configuration q is obtained as

$$Q = \mu(q)^T f \tag{4}$$

Taking into account (a) the dependence of muscle forces upon length (Equation (2)) and (b) the muscle kinematics (Equation (3)), the joint stiffness is derived by applying the chain rule to Equation (4). Symbolically, we may write:

$$R = \frac{\partial Q}{\partial q} = \mu^T \frac{\partial f}{\partial q} + \frac{\partial \mu^T}{\partial q} f. \tag{5}$$

Introducing the $N \times N$ matrix γ,

$$[\gamma]_{i,j} = \sum_{k=1}^{M} \frac{\partial^2 l_k}{\partial q_i \partial q_j} f_k. \tag{6}$$

and the $M \times M$ muscle-stiffness matrix, k,

$$[k]_{i,j} = \frac{\partial f_i}{\partial l_j}, \tag{7}$$

Equation (5) becomes:

$$R = \mu^T k \mu + \gamma. \tag{8}$$

The two terms on the right side of this expression represent, respectively, a linear transformation of the muscle-stiffness matrix and a correction term. This last term accounts for the non-linearity of the muscle-kinematics. The muscle-stiffness matrix, k, represents the *explicit* dependency of muscle tension upon muscle length.

The matrix γ represents the "geometric stiffness" induced by the muscle kinematics. Equation (6) shows that this geometric stiffness vanishes in two cases: (1) when the muscle moment-arms are constants (that is when the muscle kinematics is linear) and (2) when all the muscle operate at their rest length (that is when all the f_i's are zero). If neither condition is met, then one should assume that the geometric stiffness provides a significant contribution to the net joint-stiffness. In particular, the geometric stiffness can either increase or

decrease the margin of stability determined by the muscle-stiffness matrix.

Computational Consequences of Static Stability

The geometric stiffness plays an important role not only with respect to the control of movements and postures but also with respect to computation. In particular, here we will consider the role of static stability with respect to the equilibrium-point hypothesis (Feldman, 66; Hogan, 1984). According to this hypothesis, goal-directed movements at moderate speed are planned and implemented by the central nervous system as time-sequences of stable equilibrium postures. More formally, the equilibrium-point hypothesis can be stated as follows. The net effect of the muscles' spring-like behavior is to induce a static dependency of the joint torque, Q upon the configuration, q and upon the control input, u. That is, by combining the length-tension relations (2), the muscle kinematics (3) and tension-torque transformation (4) one obtains a single map from q and u to Q:

$$Q(q,u) = \mu(q)^T f(\phi(q),u) \quad (u \in \mathcal{U},\ q \in \mathcal{Q}). \tag{9}$$

Under precise conditions, the equilibrium equation,

$$Q(q,u) = 0 \tag{10}$$

defines a map, $g(\cdot)$ from the input, u, to an equilibrium configuration, q_0:

$$q_0 = g(u) \tag{11}$$

$$q_0 \in \mathcal{Q} \quad , \quad u \in \mathcal{U} \tag{12}$$

$$Q(q_0,u) = 0. \tag{13}$$

According to the fundamental theorem on implicit functions (Sokolnikoff & Redheffer) a necessary and sufficient condition for such a map to exist within

a region $A \subset \mathcal{Q} \times \mathcal{U}$ is that the determinant of the joint stiffness tensor, $\left|\frac{\partial Q}{\partial q}\right|$, is different from zero in A. If one of the stiffness eigenvalues changes its sign at a point P in A, so does the determinant of R and the map g ceases to be defined at P. In contrast, if all the stiffness eigenvalues remain negative in the entire region, A, then the function g is uniquely defined across that region. In this case, g maps the control variable u into a set of stable equilibria. If the control input is given as a function of time, $u(t)$, then the image of $u(t)$ under g is an *equilibrium trajectory*, that is a time sequence of stable equilibria, $q_0(t)$.

We want to stress that the above discussion refers to a multi-joint mechanisms operated by a number of actuators which may well exceed the number of joints. Thus, the geometrical value of the equilibrium-point hypothesis is given by the possibility of mapping a high-dimensional control vector, u, into a low-dimensional variable which corresponds to a configuration. Remarkably, the condition for such a transformation to exist is entirely expressed by a tensor whose rank cannot exceed the dimension of the configuration space.

Is the equilibrium point hypothesis a necessary consequence of muscles' spring-like behavior? To answer this question, one must take a closer look at equation (8) which relates the joint stiffness, R to the muscle stiffness matrix, k. The fact that muscles operate as "pulling springs" can be expressed by stating that throughout the limb configuration space the eigenvalues of the matrix $\mu^T k \mu$ are all negative. However, the net joint-stiffness matrix is also influenced by the geometric stiffness, γ which arises from the variability of the muscles' moment arms.

This geometric stiffness may generate mechanical instability within large regions of a limb's workspace. Within any such unstable regions the equilibrium-

point hypothesis is not a viable control scheme for generating movements and for maintaining limb postures. Thus, the equilibrium-point hypothesis *cannot be considered as a mere consequence of the muscles' spring like behavior*: the stability of a limb is affected by a geometrical factor which is not univocally related to the intrinsic muscle mechanics. This conclusion is illustrated by the following single-joint control example.

A Simple Example

To show how static instability can be induced by geometrical factors let us consider a simple single-joint mechanism (Figure 1): a planar pendulum operated by a pair of opposing springs (S_1 and S_2). The first spring, S_1, is a controllable element whose force-length relation is given by Hooke's law:

$$f_1 = K_1(l_1 - u) \tag{14}$$

where K_1 is the stiffness constant and u is the (controlled) rest-length. The second spring, S_2, is also governed by Hooke's law but has fixed stiffness and rest-length parameters K_2 and λ:

$$f_2 = K_2(l_2 - \lambda). \tag{15}$$

++++++++++++++++++++

FIGURE 1 NEAR HERE

++++++++++++++++++++

In the following discussion we will assume that both springs act as pulling elements and that the constants, K_1 and K_2 are negative. The springs are connected to the pendulum at a common insertion point, I. The length of

each spring is the sum of a fixed offset, L, plus a variable segment ($\overline{O_1I}$ and $\overline{O_2I}$). Hence, the muscle-kinematics is given by the equations:

$$l_1(q) = \left(\overline{OI}^2 + \overline{OO_1}^2 + 2\overline{OI}\,\overline{OO_1}cos(q)\right)^{\frac{1}{2}} + L \quad (16)$$

$$l_2(q) = \left(\overline{OI}^2 + \overline{OO_2}^2 - 2\overline{OI}\,\overline{OO_2}cos(q)\right)^{\frac{1}{2}} + L \quad (17)$$

For any pendulum configuration, q, the equilibrium condition is:

$$Q(q,u) = \mu_1(q)f_1(l_1(q),u) + \mu_2(q)f_2(l_2(q)) = 0 \quad (18)$$

where we have introduced the moment arms $\mu_1 = \frac{\partial l_1}{\partial q}$ and $\mu_2 = \frac{\partial l_2}{\partial q}$. In this simple system, with a single controlled element, the control variable, u, corresponding to each equilibrium configuration can be derived by replacing the expressions (14) and (15) for f_1 and f_2 in equation (18):

$$u(q) = l_1(q) + \frac{\mu_2(q)K_2}{\mu_1(q)K_1}(l_2(q) - \lambda). \quad (19)$$

Using equations (8) and (19), the joint stiffness at equilibrium as a function of the angle, q, is:

$$R = \mu_1^2K_1 + \mu_2^2K_2 + \underbrace{\frac{\partial \mu_1}{\partial q}f_1(q,u(q)) + \frac{\partial \mu_2}{\partial q}f_2(q)}_{\gamma}. \quad (20)$$

The last two terms on the right-hand side represent the geometric stiffness, γ, of the joint. Unlike the first two terms, they may assume a positive value and lead to a positive value of R, that is to an unstable behavior of the pendulum. This case is demonstrated in Figure 2B. The solid line represents the joint stiffness, R, at different equilibrium configurations with the following choice of geometrical and mechanical parameters: $K_1 = -1$, $K_2 = -0.8$, $\lambda = 0.4$, $\overline{OO_1} = \overline{OO_2} = \overline{OI} = 1$, $L = 0.5$. With this choice of parameters,

the equilibrium is stable ($R < 0$) at pendulum configurations ranging between 72^0 and 180^0. The joint stiffness is zero at 72^0 (Figure 2A). Between 72^0 and 0^0 the joint stiffness at equilibrium is positive. No fixed value of the control input can be used to maintain a stable posture within this latter range.

++++++++++++++++++++

FIGURE 2 NEAR HERE

++++++++++++++++++++

The solid line in Figure 2C is a plot of the control variable, u, at different equilibrium angles as derived from equation (19). This curve has a non-monotonic shape, with a maximum at 72^0. Therefore, the equilibrium configuration cannot be expressed as a single-valued function of u in the entire range of motion of the mechanism. This is a simple illustration of a case in which the equilibrium condition equation (10) cannot be used to define implicitly a map from the control input to the equilibrium configuration.[3] This result demonstrate that for a simple system operated by spring-like actuators the equilibrium-point control may not be a viable strategy for generating movements and for controlling stable postures.

However, a simple correction of the system's design may lead to a mechanical behavior that is appropriate for the equilibrium-point control. To this end, in our example (Figure 2A, dashed line) it is sufficient to move the insertion of the spring S_2 at a new point, I', which is located midway between O and I ($\overline{OI'} = \frac{1}{2}$). With this geometrical correction, the equilibrium is stable in the entire range of movement (Figure 2B, dashed line) and the control variable is a monotonic function of the equilibrium angle (Figure 2C, dashed line). In the

following sections we will apply the same approach to the anatomical analysis of the primate's upper-limb.

A Planar Model of the Monkey's Arm

In the preceding section we have discussed a specific mechanical system which may become inherently unstable by virtue of a geometrical nonlinearity. But, what if instead of such an artificially simple mechanism we were to consider a complex multi-joint system, such as a biological limb, operated by a multitude of viscoelastic elements? Is it reasonable to expect that "on the average", the spring-like properties of a large ensemble of muscles are sufficient to remove such appearingly occasional instabilities? To address these questions we have simulated the control of equilibrium postures in a more complex mechanism, which incorporated some of the biomechanical characteristics of the primate's arm. The results of our investigation demonstrate that an increase in the system complexity and in the number of spring-like actuators does not lead to better stability properties.

The Model Structure

Kinematics. We considered a 2-joint arm, restricted to move in the horizontal plane. The torso, upperarm and forearm links were modeled as rigid segments, interconnected by the shoulder and elbow joints. The relative angles of rotation were $q_1 \in [-45°, 90°]$ for the shoulder and $q_2 \in [30°, 135°]$ for the elbow. The kinematics of the model muscles were defined so as to approximate the geometry of the major arm muscles of the rhesus monkey (Table 1). A total of 17 muscles, including shoulder, elbow and two-joint flexors and extensors have been included in this model. Geometrically, each model muscle acted on a

one-dimensional line joining the attachment points. The kinematic constraint imposed by the joint was modeled as a pulley. According to the configuration of the limb, a model muscle could either act on a straight segment between the points of origin and insertion or it could be partially wrapped around the joint pulley (Figure 3).

++++++++++++++++++++++++++++++++

TABLE 1 and FIGURE 3 NEAR HERE

++++++++++++++++++++++++++++++++

The kinematics of the hand were described by a pair of cartesian coordinates, x and y, defining the position of the distal extremity of the outer link with respect to the shoulder joint. These coordinates were derived from the joint configuration, (q_1, q_2), as:

$$\begin{cases} x = l_1 \cos(q_1) + l_2 \cos(q_1 + q_2) \\ y = l_1 \sin(q_1) + l_2 \sin(q_1 + q_2) \end{cases} \tag{21}$$

where l_1 and l_2 indicate the lengths of the upperarm and of the forearm respectively.

Muscle Mechanics. Mechanically, a prominent feature of muscle behavior at steady-state is the increase of force which results both from an increase in muscle length and an increase in neuromuscular input (Rack & Westbury, 1969). This mechanical behavior is analogous to that of a tunable spring. In our model we assumed that the model muscles followed a linear length-tension relationship (Hooke's law) for each value of the control input, u, that is:

$$f = \kappa(u)\,(l - l_0(u)) \qquad u \in [0, 1]. \tag{22}$$

This is a strong simplification of the actual muscle behavior. However, data obtained by Zeffiro (1986) in the intact behaving monkey, indicate that Equation (22) may be taken as a valid first-order approximation of muscle mechanics for a wide range of muscle lengths.

The joint torque, $Q = (Q_1, Q_2)$, and the joint stiffness,

$$R = \begin{bmatrix} \frac{\partial Q_1}{\partial q_1} & \frac{\partial Q_1}{\partial q_2} \\ \frac{\partial Q_2}{\partial q_1} & \frac{\partial Q_2}{\partial q_2} \end{bmatrix}$$

are derived from the muscle stiffnesses, the muscle operating tensions and the matrix of moment arms, $[\mu(q)]_{i,j} = \frac{\partial l_i}{\partial q_j}$, as indicated by equations (4) and (5).

To derive the hand stiffness, K, corresponding to the joint stiffness, R, we took the derivative of the transformation from the joint torque, $Q = (Q_1, Q_2)$, to the hand force, $F = (F_x, F_y)$:

$$Q = J^T(q)F \tag{23}$$

where, $J(q)$, is the jacobian of the kinematic transformation (21). Thus, for those regions were $J(q)$ is invertible:

$$K = (J^T)^{-1}(R - \Gamma)J^{-1} \tag{24}$$

with

$$\Gamma = \begin{bmatrix} \frac{\partial^2 x}{\partial q_1^2}F_x + \frac{\partial^2 y}{\partial q_1^2}F_y & \frac{\partial^2 x}{\partial q_1 \partial q_2}F_x + \frac{\partial^2 y}{\partial q_1 \partial q_2}F_y \\ \frac{\partial^2 x}{\partial q_1 \partial q_2}F_x + \frac{\partial^2 y}{\partial q_1 \partial q_2}F_y & \frac{\partial^2 x}{\partial q_2^2}F_x + \frac{\partial^2 y}{\partial q_2^2}F_y \end{bmatrix} \tag{25}$$

Control. The control input to each of the model muscles was a continuous real-valued variable, u, ranging between a "resting" value (0) and a maximum-activation value (1). As indicated by Equation (22), this variable determined

uniquely the stiffness and the rest-length of the corresponding model muscle. For sake of simplicity we modeled the dependency of the stiffness and rest-length upon the input variables as linear relationships:

$$\kappa(u) = Au + B \tag{26}$$

$$l_0(u) = Cu + D. \tag{27}$$

Common sense about muscle mechanics dictates that as the activation variable increases from 0 to 1, the stiffness should increase (in absolute value) and the rest-length should decrease, corresponding to muscle shortening (Rack & Westbury, 1969; Zeffiro, 1986).

Model Parameters

The geometrical and mechanical parameters used in the model were estimated by post-mortem dissections in a rhesus monkey (Macaca mulatta). Planar projections of the arm and shoulder girdle complex were obtained by top-down x-ray imaging of the thoracic cage and arm of the monkey, fixed in a typical configuration used by alive monkeys during horizontal arm movements (Dornay, 1991a, 1991b). The torso link was modeled as an imaginary line segment connecting the two shoulder joints. The upperarm link is an imaginary line segment connecting the shoulder and elbow joints. The forearm link is the line segment passing from the elbow through the wrist till the center of the hand. The lengths of the upperarm and of the forearm links were measured to be 15.5cm and 20.2cm respectively.

The muscles listed in Table 1 were exposed and their centers of attachments were marked by drilling metal screws into the bones. The (x, y) coordinates of the muscle attachments were estimated from the x-ray projections of the

metal screws.[4] From the x-ray projections, we also estimated the radii of the model pulleys around the joints (Shoulder: 1 cm for all the muscles; Elbow, 1 cm for the flexors and 1.5 cm for the extensors). The volumes of the muscles were measured by water displacements. Table 2 lists the volumes and the coordinates of attachment for the 17 muscles used in this model.

We used these geometrical data to estimate the control parameters A, B, C and D of equations (26) and (27). These control parameters were established in three steps. First, we arbitrarily set the minimum rest-length of each muscle (D) to be 99% of its minimum physiological length (Table 2).[5] Second, we estimated the control parameters from the length-tension data obtained by Zeffiro (1986) for the triceps medialis of the intact rhesus monkey (muscle number 11 in our database). Third, we scaled these triceps parameters according to the rest-lengths and cross-sections of the other muscles. A simplified physiological cross-section, σ (An, Hui, Morrey, Linchield & Chao, 1981) was calculated for each muscle by dividing its volume by its minimum rest-length. Thus, the control parameters for all the model muscles were computed from the following expressions:

$$A_i = \frac{\sigma_i}{\sigma_{11}} \frac{D_{11}}{D_i} A_{11}$$

$$B_i = \frac{\sigma_i}{\sigma_{11}} \frac{D_{11}}{D_i} B_{11}$$

$$C_i = \frac{C_{11}}{D_{11}} D_i$$

with $i = 1, \ldots, 17$. The above equations correspond to the hypothesis that muscles are composed of sarcomeres with identical mechanical properties. On one hand, the stiffness of a muscle is directly proportional to the number of sarcomeres in parallel and inversely proportional to the number of sarcomeres

in series. On the other hand, at any level of activation, the rest-length of a muscle is given by the sarcomere's rest-length multiplied by the number of sarcomeres in series. The physiological cross-section provides an estimate of the number of sarcomeres in parallel. The number of sarcomeres in series was assumed to be proportional to the minimum rest-length, D.

++++++++++++++++++++

TABLE 2 NEAR HERE

++++++++++++++++++++

The Simulation Algorithms

To simulate the mechanical behavior of the model arm we used a software package developed by J. McIntyre on a Symbolics 3600 Lisp Machine. The software was further enhanced by the combined efforts of J. McIntyre and M. Dornay. Given a planar mechanism, this package was designed to solve both direct and inverse statics and kinematics problems. Mathematical details about the algorithms can be found in (Mussa-Ivaldi, Morasso, Hogan & Bizzi, 1991; McIntyre, 1990). Here we give a brief qualitative outline of the computational principles implemented by this software.

Direct Problems. Computationally, the arm model consists of a set of equations interacting with two types of input/output processes: the control processes and the environment. On one hand, the control processes specify a set of control variables, u_i, which determine the stiffness and rest-length of each muscle. On the other hand, the environment can act on the system either as an impedance or as an admittance. In the former case, the arm provides a position output to the environment and receives a force input from

the environment. In the latter case the input/output relations between the arm and the environment are reversed: the arm receives a position input and generates a force output. In a direct problem, the control and either the force or the position variables are specified as inputs to the arm. The problem is to determine the other variable as output to the environment. There are then two distinct types of direct problems:

- Given the control and the force variables, determine the position variable. A particular case of this problem is that of finding the equilibrium position corresponding to a given control pattern. In this case, it is implicitly assumed that the environment imposes a constraint of zero force on the model arm.

- Given the control and the position variables, determine the force variable. An example is the problem of finding the force exerted by the hand at a workspace location with a given set of control inputs. A strictly related direct problem is that of determining the stiffness tensor corresponding to given control and position variables.

One important aspect of these direct problems is that they are all well-posed- that is they can be uniquely solved- regardless of the redundancy of degrees of freedom in the model arm.

Inverse Problems and the Backdriving Algorithm. Inverse problems arise when one tries to determine the control variables corresponding to given values of both force and position variables at the interface with the environment. For a redundant system such as our model arm, these inverse problems are ill-posed and their solution is not unique. For example, consider the

problem of finding the control variables corresponding to a given equilibrium position of the arm. In this case both the position and the force (zero) at the interface with the environment are specified. It is evident that with a redundant system of muscles, there are infinite patterns corresponding to the same equilibrium position. In order to derive a unique solution it is necessary to impose some extra constraint, such as an optimization principle.

Our software implemented a specific optimization principle, the *backdriving* algorithm which corresponded to a process of adaptive control. Briefly, backdriving the arm from a current equilibrium position to a new equilibrium position is equivalent to performing the following two steps: 1) impose a passive displacement of the arm to the new position and 2) reset the control variables so as to eliminate the induced elastic forces. Clearly, in the passive displacement the system moves to a configuration of minimum potential energy. Then, the active change (step 2) is equivalent to finding the input pattern which minimizes the change in potential energy with respect to the previous equilibrium.

The Model Arm Has Unstable Behaviors

To investigate the stability of our model arm, we started by setting all the control parameters (Equations (26) and (27)) to the same value (0.5). With these control parameters, the arm was at equilibrium in the position shown in Figure 4-A. Then, while keeping constant the control inputs, we calculated the joint stiffness as a function of the hand location in the workspace.[6] The dark dots in Figure 4 indicate locations at which the joint stiffness was unstable. The light dots indicate locations at which the stiffness was stable. It is apparent that with this choice of parameters there was a significant region of

instability. Similar unstable regions were observed with other control patterns.

++++++++++++++++++++

FIGURE 4 NEAR HERE

++++++++++++++++++++

Next, we considered the effect of varying the degree of muscle coactivation upon the size of the unstable region. Figures 4-B and 4-C, show the regions of instability with all the control parameters equal to 0.2 and 0.8 respectively. As the degree of coactivation increased, so did the region of instability. Contrary to what one might have expected, *coactivation made the limb more unstable.* This counterintuitive finding is explained by observing that the essential source of instability for the arm is the geometric stiffness, γ, in equation (8). Since muscles always pull ($f_i < 0$), the sign of the components of γ (see equation(6)) can be either positive or negative according to the sign of the derivatives of the moment arms, $\frac{\partial^2 l_k}{\partial q_i \partial q_j}$. If these derivatives are negative, then the corresponding contributions to γ are positive and the stability margin is decreased. By increasing the activation of a muscle whose moment-arm derivative is negative the margin of stability is further reduced.

Summing up our results indicate that a) with all the tested values of the control parameters, the model arm had a wide region of instability; b) the region of instability was increased by increasing the level of coactivation. This unstable behavior had a dramatic impact on the possibility to map a desired equilibrium location into a set of control variables- that is on the possibility of implementing an equilibrium-point control. Using the backdriving algorithm, we tried to set the arm at a number of new equilibrium locations (locations

a, b, c, d and e in Figure 4-A). The algorithm succeeded in finding the control patterns for the locations a and e, which fell within the stability region. However, it failed to find the appropriate controls for the positions b, c and d which lied inside the unstable region.

Stability Can Be Achieved by Simple Geometrical Modifications

Our first approximation of the monkey's arm geometry, led us to a model with unstable behaviors. This instability is not only undesirable for the equilibrium-point control but it is also scarcely plausible in physiological terms: primates are capable of maintaining stable arm postures even after deafferentation (Taub, Goldberg & Taub, 1975; Bizzi et al, 1984). If stability is an important functional requirement, then it is possible to proceed in one of two alternative directions: 1) with the current model structure, try to choose only those motor commands which ensure postural stability or 2) modify the model structure in such a way that any motor command is guaranteed to generate a stable posture. The first approach leads to the complex (and not always possible) task of implementing ad hoc computational procedures capable of avoiding unstable control patterns. In contrast, the second approach relieves the motor controller from such a computational burden.

In order to correct the structure of the model, we examined the contribution of each muscle to the joint stiffness matrix, R. In our model, two conditions were always satisfied by the joint-stiffness matrix, R: 1) R was symmetric ($R_{1,2} = R_{2,1}$),[7] and and 2) The diagonal stiffness terms, $R_{1,1}$ and $R_{2,2}$, were larger (in absolute value),[8] than the two-joint term, $R_{1,2}$. If the above two conditions are satisfied, it can be proved (Dornay, 1991a) that *a necessary and sufficient condition for a stable joint stiffness is having stable (or negative)*

diagonal components, ($R_{1,1} < 0$ and $R_{2,2} < 0$). Therefore we only needed to consider the contributions of the muscles to the two diagonal components, $R_{1,1}$ (shoulder stiffness) and $R_{2,2}$ (elbow stiffness). Making use of Equation (5), these components can be expressed as

$$\begin{cases} R_{1,1} = \sum_{i=1}^{17} r_{1,i} \\ R_{2,2} = \sum_{i=1}^{17} r_{2,i} \end{cases} \tag{28}$$

where we have introduced the *angular muscle stiffnesses*

$$\begin{cases} r_{1,i} = \mu_{1,i} \frac{\partial f_i}{\partial q_1} + \chi_{1,i} f_i \\ r_{2,i} = \mu_{2,i} \frac{\partial f_i}{\partial q_2} + \chi_{2,i} f_i \end{cases} \tag{29}$$

with

$$\chi_{i,1} = \frac{\partial \mu_{1,i}}{\partial q_1}$$
$$\chi_{i,2} = \frac{\partial \mu_{2,i}}{\partial q_2}.$$

The angular stiffnesses summarizes the contribution of each muscle to the shoulder and elbow joint stiffness. The coefficients, $\chi_{1,i}$ and $\chi_{2,i}$ play a major role in establishing the margin of stability of a muscle.

This point is illustrated in Figure 5 which shows the variation of the parameters related to the muscle pectoralis major capsularis, as the shoulder angle changes from -45^0 to 90^0. The model geometry of this particular muscle is also illustrated in Figure 3. The top-left panel of Figure 5 shows the plots for the muscle length, l, the moment-arm, $\mu = \frac{\partial l}{\partial q}$, and the coefficient $\chi = \frac{\partial \mu}{\partial q}$. In the first part of the shoulder-joint range, $q \in [-45^0, +11^0]$, the muscle is wrapped around the joint-pulley (Figure 3). Accordingly, the moment-arm is constant and $\chi = 0$. In this initial range the force and the torque change

linearly and the angular stiffness is constant and negative. The muscle contributes to stability. When the muscle becomes unwrapped from the pulley, the moment arm starts suddenly to increase (in absolute vaue) and χ jumps to a large negative value. At this point, the tension developed by the muscle is sufficiently large to induce a positive angular stiffness, for all the values of the control input. The muscle contributes to instability. As the joint angle keeps increasing, the rate of change of the moment arm and the muscle tension decrease. At $q = 48^0$ the geometric stiffness contributed by χf becomes smaller than the "intrinsic stiffness", $\mu \frac{\partial f}{\partial q}$. As a consequence, the muscle contributes again to joint stability between 48^0 and 90^0.

++++++++++++++++++++

FIGURE 5 NEAR HERE

++++++++++++++++++++

A simple geometric modification that was sufficient to eliminate the instability of pectoralis major scapularis is shown in Figure 6. We changed the effective origin and insertion so as to keep the muscle in closer proximity to the joint. As shown in Figure 7, with this modification, the moment arm remains constant for a larger range. As the muscle becomes unwrapped, the muscle tension is small enough to maintain the angular stiffness at a negative value. Remarkably, this modification corresponded to a closer similarity between the model arm and the actual musculoskeletal geometry. Real muscle, such as the pectoralis major, do not connect the actual attachment points in a straight line, as we supposed in the initial model. Instead, connective tissues constrain the line of action of a muscle and shift its effective origin and insertion towards

the center of the joint, a situation that is captured by the modified geometry of Figure 6.

Interestingly, this analysis provides a rationale for the apparent lack of efficiency of the biological design. By keeping the muscles close to a joint, their mechanical advantage is reduced. However, at the same time the stability range is substantially increased.

++++++++++++++++++++++++++

FIGURES 6 and 7 NEAR HERE

++++++++++++++++++++++++++

We repeated the above stability analysis for all the 17 muscles in the model. Then, we modified the effective origins and insertions of these muscles so as to ensure joint stability for every possible value of the control inputs. With this modification, the instable regions of Figure 4 were completely removed. As a consequence, the backdriving algorithm became successful in deriving a control pattern for any desired equilibrium position. For example, Figure 8 shows the outcome of the backdriving algorithm as the hand posture was smoothly shifted from an initial to a final position (Figure 8-A and 8-B). This equilibrium-point trajectory transversed a region that was unstable before the geometric modification of the model muscles. The control signals corresponding to the equilibrium-trajectory are shown in Figure 8-C. In this as in all other tested trajectories, each signal varied continuously from an initial to a final value. Thus, by removing the instabilities from the model arm it was possible to establish a continuous mapping between equilibrium positions and muscle-control variables.

++++++++++++++++++++

FIGURE 8 NEAR HERE

++++++++++++++++++++

Summary and Conclusions

We have investigated the relation between static stability of a limb and the equilibrium-point hypothesis. Mathematically, the equilibrium-point control is equivalent to the establishing of a mapping between the command signals delivered to the muscles and the equilibrium configurations of a limb. A condition for this mapping to be possible is that the limb is stable across the workspace or, more precisely, that the limb's stiffness has only negative eigenvalues. We analyzed how this conditions may be translated into precise biomechanical constraints for single- and multi-joint limbs.

Our results indicate that the viscoelastic properties of the muscles do not provide a sufficient condition for the equilibrium point hypothesis to be applicable. In fact, one can design single- and multi-joint systems having inherent unstable behaviors in spite of the fact that they are operated by viscoelastic muscle-like actuators. The instability of such systems arises from the fact that the moment-arms of the actuators about the joints depend upon the joint angles. This variable moment arms introduce an unstable stiffness component which may overshadow the stability provided by the viscoelastic properties of the actuators.

We studied the relations between limb stability and biomechanical constraints by developing a computer model of the primate's arm. We adopted a commonly used simplification of muscular geometry: each model muscle

acted along a straight line joining the centroid of the origin to the centroid of the insertion (Amis, Dowson & Wright, 1979). Clearly, this geometrical representation is just a coarse approximation of the actual muscle kinematics. However, it provided us with a model in which the muscles's moment arms changed as a function of the joint angles in the same direction as the actual muscles's moment arms. For this reason, the straight-line geometry constitutes a significant improvement with respect to the more commonly adopted assumption of constant moment arms.

We estimated the origins and insertions of the model muscles by dissection and x-ray imaging of 17 arm muscles in a rhesus monkey. Then we simulated the stability of the arm model with a variety of command inputs. Our results indicated that the straight-line muscle kinematics lead to the postural instability of the model arm in a large region of the arm's workspace. Remarkably, this instability was neither removed, nor reduced by muscle coactivation. On the contrary, we found that muscle coactivation increased the region of instability. One, and perhaps the only, effective way to remove instability from our model was to modify the effective origins and insertions of the model muscles. More specifically, this modification corresponded to approximate the mechanical action of the tendons and of the connective tissues which in the actual arm keep the muscles in the proximity of the joints. This result suggests that a simple design constraint rather than a dedicated control process is sufficient to ensure stability to the limb. One should observe that the same design factor which ensures stability- the closeness of the muscles to the joints- is also responsible for a decrease of the joint torque that a muscle can generate. Thus, we believe that we have found a rationale for an apparent lack of "efficiency"

in the biological design.

The elimination of the possible sources of instability in the mechanical structure of the arm is crucial for solving the computational problems associated with the equilibrium-point hypothesis. For example, we considered the task of deriving a pattern of muscle activations which generates a desired equilibrium configuration of the arm. With a set of 17 muscles, this problem was severely ill-posed: the same equilibrium configuration could be achieved by infinite patterns of muscle activations. A solution to this problem can be found by minimizing the changes in potential energy associated with the transition to a new posture (Mussa-Ivaldi, Morasso & Zaccaria 1988; Mussa-Ivaldi et al., 1991). Our results indicate that this minimum-energy principle can effectively be implemented by a simulation algorithm only after all sources of instability have been removed from the anatomical model. The inability to derive appropriate command patterns in the presence of structural instabilities is a further demonstration of the crucial role played by the biological design with respect to information processing in motor control.

Notes

1. A system is said to be statically conservative when the generalized force at rest can be expressed as the gradient of a scalar potential function, $U(q)$. This condition is equivalent to requiring that $\frac{\partial Q_i}{\partial q_j} = \frac{\partial Q_j}{\partial q_i}$.

2. This is a direct consequence of Stokes' theorem. A non-symmetric stiffness corresponds to a force field with non-zero curl. According to Stokes' theorem, the work around a close path is given by the net flux of the field's curl across the surface enclosed by the path.

3. In this case, the fact that the opposite map (from equilibrium angle to input) is defined is merely a consequence of the lack of redundancy in this ad-hoc example: there is a single configuration variable and a single controlled element. If there were more controlled elements than configuration variables (as is the case with musculoskeletal systems) the mapping between q and u would have been ill-defined in both directions.

4. Each model link connected a proximal joint with a distal joint. A muscle's origin was referred to a Cartesian system centered at the distal joint. A muscle's insertion was referred to a Cartesian system centered at the proximal joint. For both Cartesian systems, the x axis included the segment joining the proximal to the distal joint (the link axis) and was oriented from proximal to distal. When all the joint angles were 0 degrees, the y axes were all parallel and pointed to the anterior direction. For a more detailed account of the attachment geometry see Dornay (1991a).

5. That is, the minimum length which could be assumed across the workspace.

This setting assured that the muscle always had some (small) residual tension.

6. A necessary and sufficient condition for hand stability at equilibrium is that the joint stiffness is stable (Dornay, 1991b).

7. The symmetry is derived from the fact that there are no control coupling between muscles spanning different joints. For proof see Dornay (1991b).

8. This feature was in agreement with the joint stiffness matrices measured in human subjects (Mussa-Ivaldi et al., 1985; Flash & Mussa-Ivaldi, 1990).

REFERENCES

Amis, A. A., Dowson, D., & Wright, W. (1979). Muscle strengths and musculoskeletal geometry of the upper limb. *Engng Med.*, 8, 41–48.

An, K. N., Hui, F.C., Morrey, B. F., Linchield, R. L., & Chao, E. Y. (1981). Muscles across the elbow joint: a biomechanical analysis. *J. Biomechanics*, 14, 659–669.

Bizzi, E., Accornero, N., Chapple W., & Hogan, N. (1984). Posture control and trajectory formation during arm movement. *J. of Neuroscience*, 4, 2738–2744.

Colgate, J. (1988). *The control of dynamically interacting systems.* PhD thesis, Department of Mechanical Engineering, MIT,

Colgate, J., & Hogan, N, (1989). An analysis of contact instability in terms of passive physical equivalents. *IEEE Proc. International Conference on Robotics and Automation*, pp. 404–409.

Dornay, M. (1991a). Static analysis of posture and movement, using a 17-muscle model of the monkey's arm. *ATR Technical Report TR–A–0109.*

Dornay, M. (1991b). Control of movement, postural stability, and muscle angular stiffness. *Proc. IEEE System Man and Cybernetics*, Charlottesville Virginia, USA, pp. 1373–1379.

Feldman, A. G. (1966). Functional tuning of nervous system with control of movement or maintenance of a steady posture. III. Mechanographic analysis of the execution by man of the simplest motor task. *Biophysics*, 11, 766–775.

Flash, T, & Mussa-Ivaldi, F. A. (1990). Human arm stiffness characteristics during the maintenance of posture. *Exp. Brain. Res.*, 82, 315–326.

Hogan, N. (1984). An organizing principal for a class of voluntary movements. *Journal of Neuroscience*, 4, 2745–2754.

Kelso, J. A. S. & Holt, K. G. (1980), Exploring a vibratory system analysis of human movement production. *J. of Neurophysiology*, 43, 1183–1196.

McIntyre, J. (1990). *Utilizing elastic system properties for the control of posture and movement.* Ph.D. Thesis, Dept. of Brain and Cognitive Sciences, MIT.

Mussa-Ivaldi, F., Hogan, N., & Bizzi, E. (1985). Neural, mechanical and geometric factors subserving arm posture in humans. *J. of Neuroscience*, 5, 2732–2743.

Mussa-Ivaldi, F. A., Morasso, P., & Zaccaria, R. (1988). Kinematic networks: a distributed model for representing and regularizing motor redundancy. *Biological Cybernetics*, 60, 1–16.

Mussa-Ivaldi, F. A., Morasso, P., Hogan, N., & Bizzi, E. (1991). Network models of motor systems with many degrees of freedom. In M. D. Fraser (Ed.), *Advances in control networks and large scale parallel distributed processing models.* Ablex Publishing Corporation, Norwood, N.J.

Ogata, K. (1970). *Modern control engineering.* Engineering Series. Prentice–Hall, Inc., Englewood Cliffs, NJ.

Rack, P. M. H., & Westbury, D. R. (1969). The effects of length and stimulus rate on tension in isometric cat soleus muscle. *Journal of Physiology*, 204, 443–460.

Taub, E, Golberg, I. A., & Taub, P. (1975). Deafferentation in monkeys: pointing at a target without visual feedback. *Exp. Neurol.*, 46, 178–186.

Sokolnikoff, I. S, & Redheffer, R. M. (1966). *Mathematics of physics and modern engineering*, Mc Graw Hill.

Zeffiro, T. A. (1986). *Motor adaptations to alterations in limb mechanics.* Ph.D. Thesis, Dept. of Brain and Cognitive Sciences, MIT.

Table 1. The Dissected Muscles

#	Muscle	Origin	Insertion	Function
1	Latissimus Dorsi	Vertebrae	Humerus	Shoulder Extensor
2	Posterior Deltoid	Scapula	Humerus	Shoulder Extensor
3	Teres-Major	Scapula	Humerus	Shoulder Extensor
4	Teres-Minor	Scapula	Humerus	Shoulder Extensor
5	Infra-Spinatus	Scapula	Humerus	Shoulder Extensor
6	Pectoralis Major Capsularis	Clavicula	Humerus	Shoulder Flexor
7	Pectoralis Major Sternalis	Sternum	Humerus	Shoulder Flexor
8	Anterior Deltoid	Clavicula	Humerus	Shoulder Flexor
9	Coraco Brachialis	Scapula	Humerus	Shoulder Flexor
10	Triceps Lateralis	Humerus	Ulna	Elbow Extensor
11	Triceps Medialis	Humerus	Ulna	Elbow Extensor
12	Brachialis	Humerus	Ulna	Elbow Flexor
13	Brachio-Radialis	Humerus	Radius	Elbow Flexor
14	Pronator Teres	Humerus	Radius	Elbow Flexor
15	Triceps Longus	Scapula	Ulna	2-Joint Extensor
16	Biceps Brevis	Scapula	Radius	2-Joint Flexor
17	Biceps Longus	Scapula	Radius	2-Joint Flexor

Table 2. Muscle Parameters.

	Muscle	Origin (cm)	Insertion (cm)	Volume (cm^3)	D (cm)
1	Latissimus Dorsi	(-5.5, -10.0)	(2.1, 1.0)	50.0	11.9
2	Posterior Deltoid	(0.8, -4.4)	(5.2, 1.5)	21.3	4.28
3	Teres-Major	(-0.2, -6.4)	(2.8, 0.5)	25.3	5.35
4	Teres-Minor	(0.2, -5.0)	(0.8, 0.6)	4.75	4.87
5	Infra-Spinatus	(-0.2, -4.8)	(0.8, 0.6)	26.4	4.76
6	Pectoralis Major Capsularis	(-4.8, -0.8)	(2.7, 1.5)	37.0	4.76
7	Pectoralis Major Sternalis	(-5.5, 1.3)	(2.7, 1.5)	33.0	4.19
8	Anterior Deltoid	(-2.4, -2.0)	(5.2, 1.5)	15.1	7.18
9	Coraco Brachialis	(-1.6, -1.0)	(6.0, 1.5)	4.3	6.90
10	Triceps Lateralis	(-12.2, 0.2)	(-0.8, -1.6)	45.8	12.3
11	Triceps Medialis	(-5.6, -0.2)	(-0.8, -1.6)	26.5	5.86
12	Brachialis	(-5.7, 0.7)	(2.3, -0.3)	15.2	4.39
13	Brachio-Radialis	(-5.0, -0.2)	(16.5, 0.8)	24.4	13.3
14	Pronator Teres	(-1.2, -0.5)	(9.3, 0.3)	9.5	8.76
15	Triceps Longus	(0.4, -2.2)	(-0.8, -1.6)	45.8	13.6
16	Biceps Brevis	(-1.6, -1.0)	(2.7, 0.5)	28.0	14.0
17	Biceps Longus	(-0.73, -1.5)	(2.7, 0.5)	26.5	14.6

Figure Captions

Figure 1. A planar pendulum operated by a pair of opposing springs. q is the joint angle of the pendulum.

Figure 2. Stability analysis of the planar pendulum. R is the joint stiffness, and u is the control input to the tunable (left) spring. The solid lines show that the system is not stable for joint angles from 0^0 to 72^0. The dashed lines show that the system becomes stable when the attachment of the right spring is moved from I to I'.

Figure 3. Initial geometric model of the shoulder flexor muscle pectoralis major capsularis. The muscle originates from the torso link at **a**. The insertion of the muscle to the upperarm link is marked as **b** ($q = -45^0$) or **c** ($q = 90^0$). The joint angle affects the muscle length and whether it is wrapped around its pulley at the joint (**b**) or is unwrapped (**c**).

Figure 4. Initial hand stability. When the control input to each muscle was 0.5, the hand was stable at the equilibrium position shown in panel **A**. (**S** marks the shoulder joint, **E** the elbow, and the big open circle shows the hand position). This equilibrium position was used as a starting point for simulating various hand movements. Using the backdriving algorithm, the hand could be moved to points **a** and **e**, but not to points **b**, **c** and **d**. The failure was because the hand stiffness became unstable during these movements. To get an insight, we plotted the joint stiffness as a function of the hand location in the workspace. **A**: all the control inputs are 0.5. **B**: all the control inputs are 0.2. **C**: all the control inputs are 0.8. The dark dots indicate locations where the joint stiffness is unstable, while the light dots indicate stable locations.

Figure 5. Initial stability analysis of pectoralis major capsularis. A flexion movement is shown in which the shoulder angle changes from -45^0 to 90^0. In the **Geometry** panel, the muscle length, l, decreased from 8.7 cm to 4.8 cm. The moment arm of the muscle around the shoulder joint, μ, was initially constant at -1 cm $*$ radian^{-1}, but at $q = 11^0$ it started to decrease, eventually reaching its final value of -2.9 cm $*$ radian^{-1}. The moment arm derivative,χ, was zero at the first stage of the movement, jumped to -1.8 cm $*$ radian^{-2} at $q = 11^0$, and then started to increase, reaching a final value of -0.75 cm $*$ radian^{-2}. In the **Force, Torque** and **Stiffness** panels, the behavior of the muscle is shown for six different control inputs u.

Figure 6. Stabilized geometric model of the shoulder flexor muscle pectoralis major capsularis. The initial geometric model was described in Figure 3. The muscle's line of action is constrained by connective tissues represented by the effective origin **d** and the effective insertion **e** or **f**.

Figure 7. Final stability analysis of pectoralis major capsularis. The same analysis described in Figure 5 was repeated using the "corrected" geometry shown in Figure 6. The muscle length, l, decreased from 9.1 cm to 6.7 cm. The moment arm of the muscle around the shoulder joint, μ, was initially constant at -1 cm $*$ radian^{-1}, but at $q = 70^0$ it started to decrease, eventually reaching its final value of -1.2 cm $*$ radian^{-1}. The moment arm derivative,χ, was zero at the first stage of the movement, jumped to -0.5 cm $*$ radian^{-2} at $q = 70^0$, and then started to increase, reaching a final value of -0.39 cm $*$ radian^{-2}.

Figure 8. A typical equilibrium-point trajectory. The chosen hand path is a straight line with 26 intermediate points. A control input to the 17 muscles is specified for each intermediate point, defining it as an equilibrium point. The neural control input profiles for all the muscles is very smooth. When the input to a muscle reaches a minimum (0) or a maximum (1), it stays there as long as the backdriving algorithm expects it to decrease or increase, respectively. In this case other muscles take over and produce the needed change in torque. The 13th muscle shows this behavior in the middle of the movement. **S** = shoulder, **E** = elbow, **D** = double joint muscle, **e** = extensor, **f** = flexor muscle. The serial numbers refer to Table 1 and Table 2.

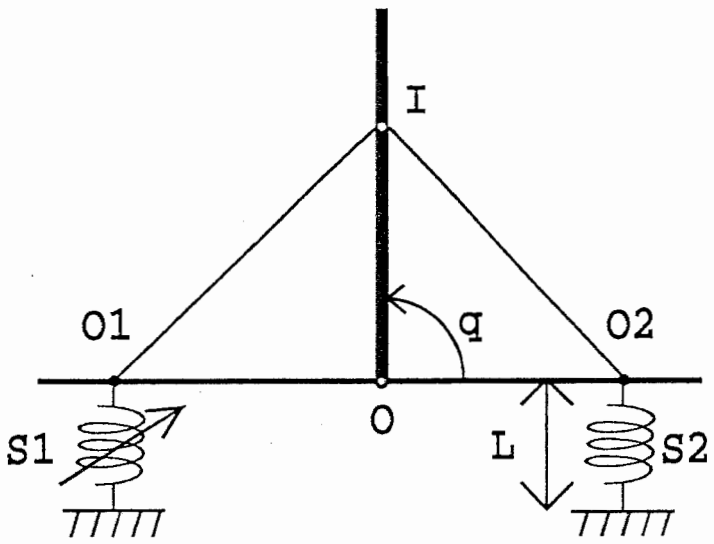

Figure 1

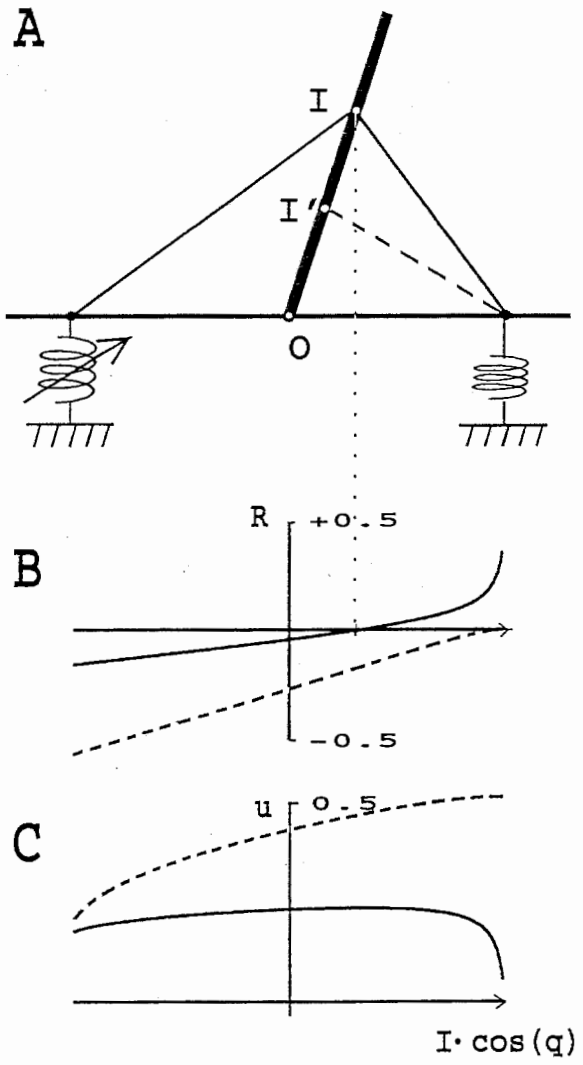

Figure 2

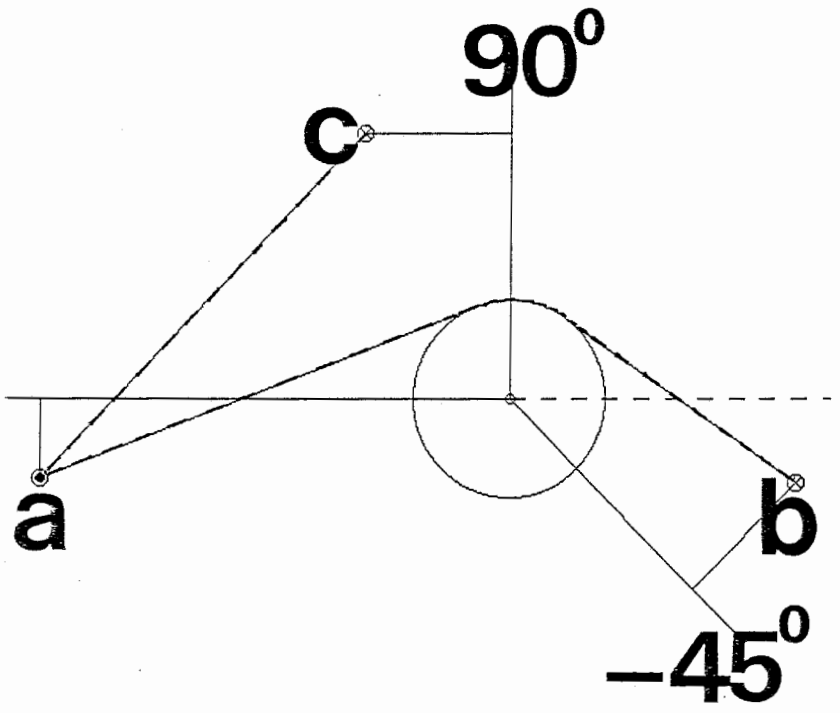

Figure 3

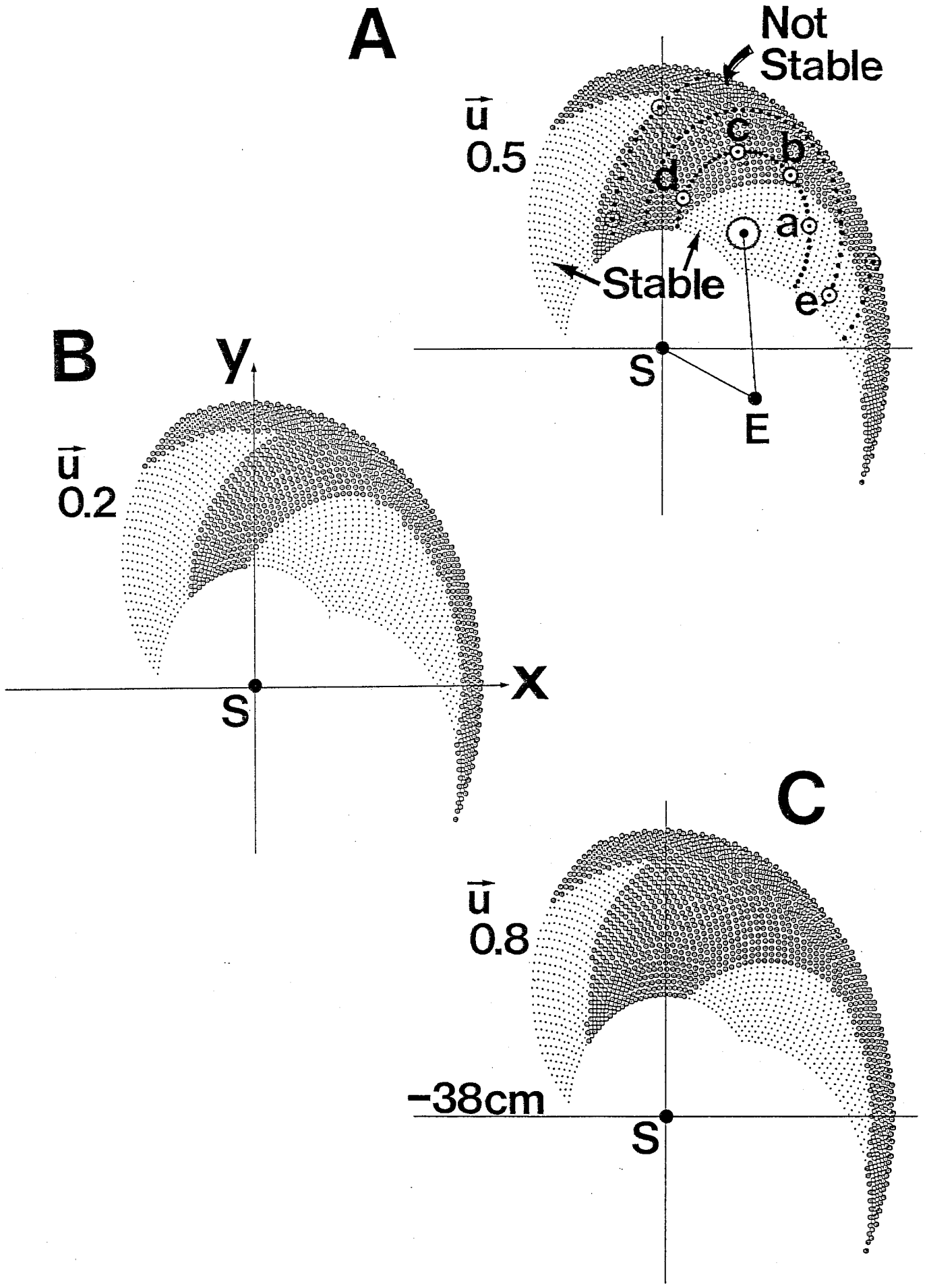

Figure 4

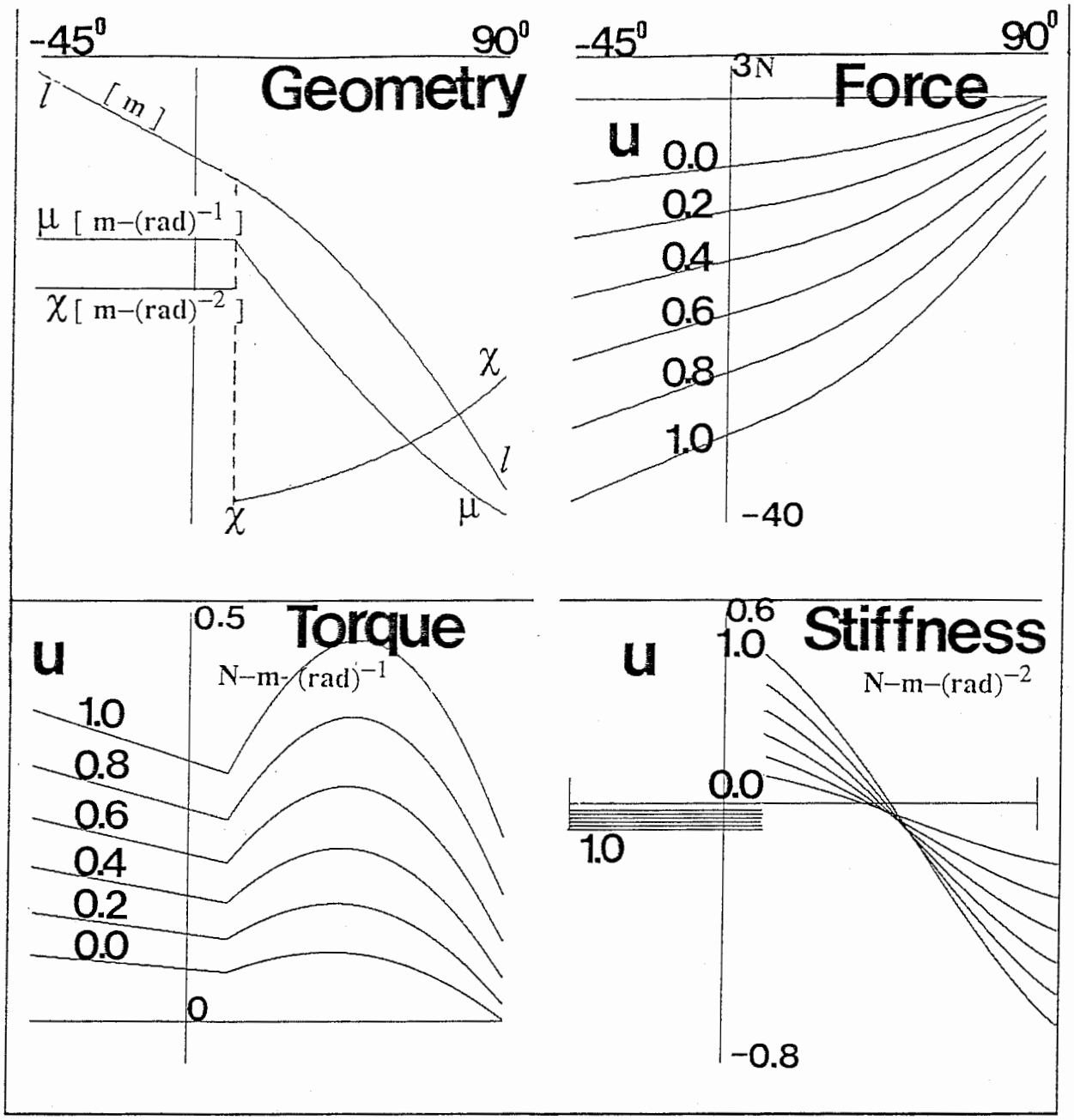
-45⁰
90⁰
Geometry
l [m]
μ [m–(rad)⁻¹]
χ [m–(rad)⁻²]
χ
l
μ
-45⁰
90⁰
3N
Force
u
0.0
0.2
0.4
0.6
0.8
1.0
-40
0.5
Torque
u
N–m–(rad)⁻¹
1.0
0.8
0.6
0.4
0.2
0.0
0
0.6
1.0
Stiffness
u
N–m–(rad)⁻²
0.0
1.0
-0.8

Figure 5

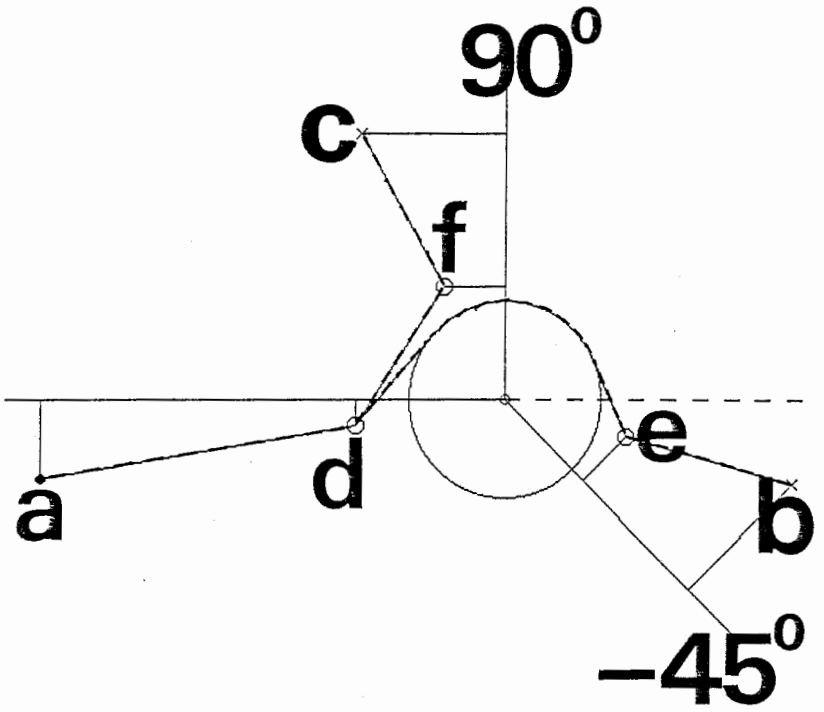

Figure 6

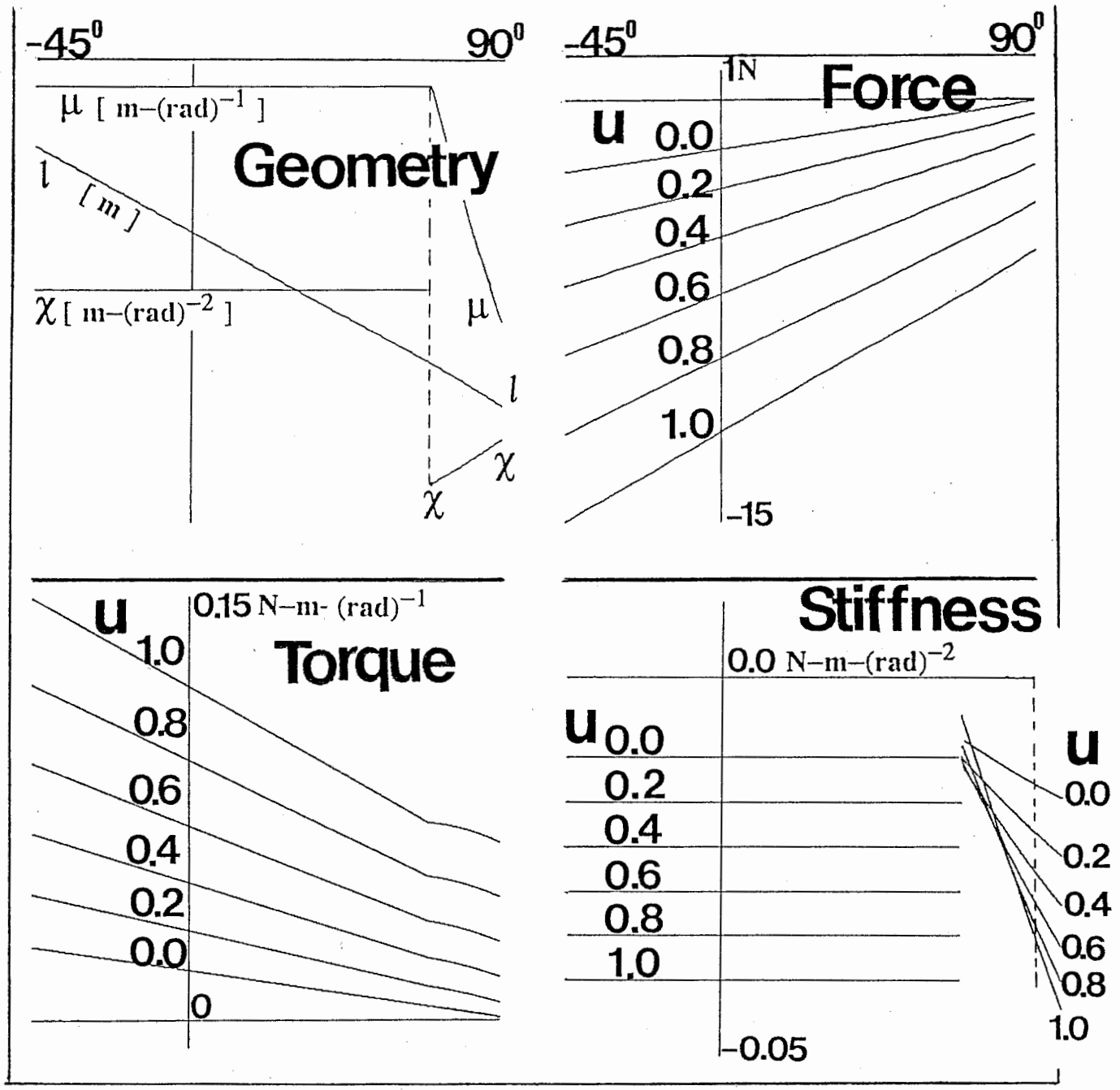
-45⁰
90⁰
μ [m–(rad)⁻¹]
Geometry
l [m]
χ [m–(rad)⁻²]
μ
l
χ
χ
-45⁰
90⁰
1N
Force
u
0.0
0.2
0.4
0.6
0.8
1.0
-15
u
1.0
0.8
0.6
0.4
0.2
0.0
0.15 N–m- (rad)⁻¹
Torque
0
Stiffness
0.0 N–m–(rad)⁻²
u
0.0
0.2
0.4
0.6
0.8
1.0
-0.05
u
0.0
0.2
0.4
0.6
0.8
1.0

Figure 7

A

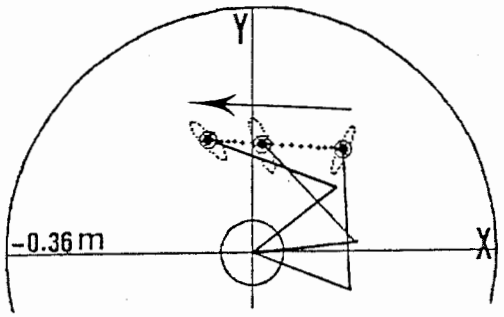
Y
-0.36 m
X

B

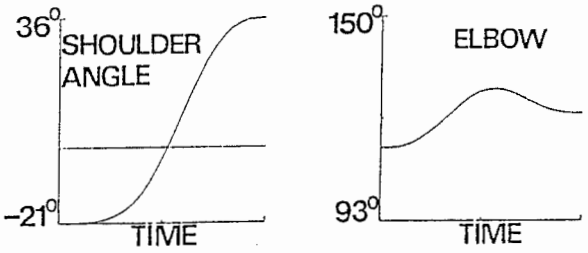
36°
SHOULDER
ANGLE
-21°
TIME
150°
ELBOW
93°
TIME

C

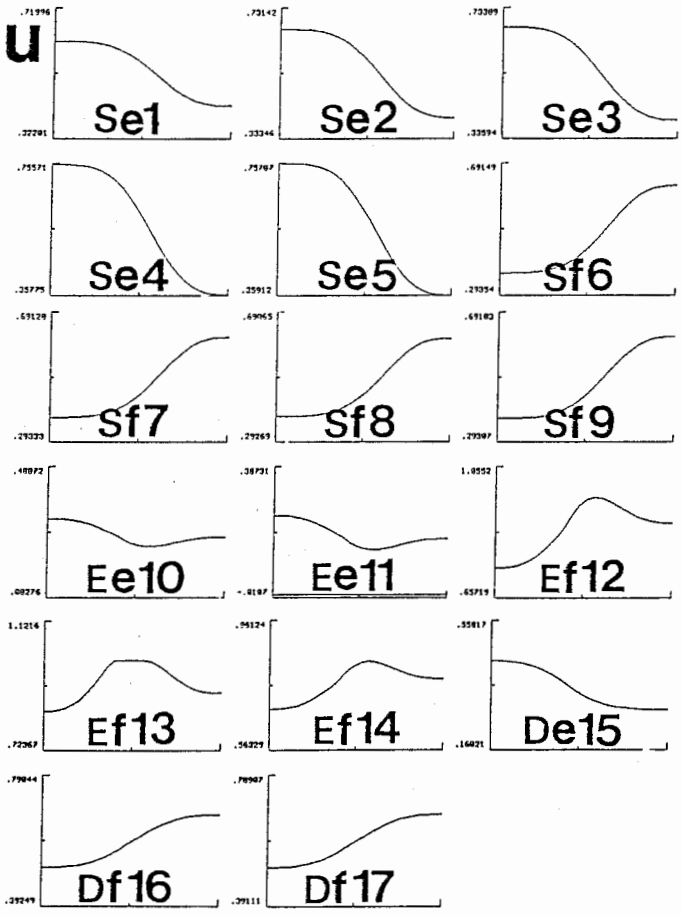
u
Se1
Se2
Se3
Se4
Se5
Sf6
Sf7
Sf8
Sf9
Ee10
Ee11
Ef12
Ef13
Ef14
De15
Df16
Df17

Figure 8